# Combining Turbulence and Mud Rheology in a Conceptual 1DV Model – An advanced continuous modeling concept for fluid mud dynamics

*Oliver Chmiel[1], Marie Naulin[2] and Andreas Malcherek[1]*

*[1] University of the German Armed Forces, Institute of Hydromechanics and Hydraulic Engineering, Munich, oliver.chmiel@lfu.bayern.de*
*[2] Federal Waterways Engineering and Research Institute (BAW), Hamburg*

## Summary

Fluid mud influences the tidal dynamics of estuaries. Predictive engineering tools are required for maintenance strategies of estuaries to minimize siltation and lower the economic and ecological costs. Therefore, the non-Newtonian flow behavior of fluid mud has to be considered in numerical models. In this paper, an advanced modeling method is presented in order to simulate the entire depth in an estuary (from clear water to immobile bed) with one model. Within this modeling concept the momentum and the concentration balance equations are solved together with a $k$-$\omega$-turbulence model continuously over the entire water column including the fluid mud bottom. In order to achieve this objective, the effective viscosity in the momentum equation has to represent turbulence in the water column and the rheology of mud in the fluid mud bottom. The $k$-$\omega$ turbulence model is interpreted in a new way, so that it could be applied for fluid mud layers where no turbulence is produced. The viscoplastic, shear thinning behavior of fluid mud is represented by the rheological model of Malcherek and Cha (2011). The rheological viscosity was parameterized for varying shear rate, grain size, and volume solid content. The rheological formulation accounts for a yield stress dependency on the volume solid content and for flocculation. Modeling results of a vertical 1D model are presented describing turbulent and rheological flow equally for the fluid and the solid phase. The formation of a fluid mud layer is shown by vertical velocity and concentration profiles.

## Keywords

fluid mud, mud rheology, effective viscosity, suspended solids concentration, turbulence damping

## Zusammenfassung

*Flüssigschlick beeinflusst die Tidedynamik der Ästuare. Für die Entwicklung von Unterhaltungsstrategien an Ästuaren werden vorausschauende Methoden und Werkzeuge benötigt, um die Verschlickung zu minimieren und die ökonomischen und ökologischen Kosten zu reduzieren. Hierfür ist es erforderlich, dass das nicht-Newtonsche Fließverhalten von Flüssigschlick in den numerischen Modellen berücksichtigt wird. In dieser Veröffentlichung wird ein neuer Modellansatz präsentiert, der es ermöglicht die gesamte Tiefe in einem Ästuar (vom klaren Wasser bis zum unbeweglichen Boden) mit einem Modell zu simulieren. In* *diesem Modellkonzept wird die Impulsgleichung und die Transportgleichung zusammen mit einem $k$-$\omega$-Turbulenzmodell kontinuierlich über die gesamte Wassersäule bis hin zum Flüssigschlickboden gelöst. Um dieses Ziel zu erreichen, wird eine effektive Viskosität in der Impulsgleichung eingeführt, die sowohl die Wirkung von Turbulenz im freien Wasser als auch die Rheologie von Flüssigschlick am Boden wiedergibt. Das $k$-$\omega$-Turbulenzmodell wird neu interpretiert, so dass es auch im Flüssigschlick, in dem keine Turbulenz produziert wird, angewandt werden kann. Das viskoplastische, scherverflüssigende Verhalten von Flüssigschlick wird durch das rheologische Modell von Malcherek und Cha (2011) beschrieben. Die rheologische Viskosität wird dabei durch die Scherrate, den Korndurchmesser und den Feststoffgehalt parametrisiert. Dieses rheologische Modell berücksichtigt eine Fließgrenze, die vom Feststoffgehalt abhängig ist, sowie Flockulation. Die Simulationsergebnisse eines vertikalen 1D-Modells beschreiben die turbulente und rheologische Strömung gleichermaßen für die flüssige wie für die feste Phase. Die Bildung einer Flüssigschlickschicht wird durch vertikale Geschwindigkeits- und Konzentrationsprofile nachgewiesen.*

## Schlagwörter

*Flüssigschlick, Rheologie, Effektive Viskosität, Schwebstoffgehalt, Turbulenzdämpfung*

## 1 Introduction

Fluid mud is a high concentrated aqueous suspension of fine-grained sediment and organic matter. It is often associated with a lutocline, a sudden change in sediment concentration with depth. Fluid mud typically forms in near-bottom layers in lakes and estuaries, but it can occur in any water body with sufficient fine-sediment supply and periods of low intensity flow.

The occurrence of fluid mud is often leading to high maintenance costs of waterways such as estuaries, e. g. for dredging, prevention of pollutant propagation and nature conservation. In Germany in particular, the Ems Estuary is affected by fluid mud: fine-sediment concentrations up to 300 kg/m³ and fluid mud layers up to a thickness of 2 m were measured (Schrottke 2006). Additionally, the occurrence of high concentrated suspended solids may lead to ecological problems in the estuary, such as increased oxygen demand due to absorbed organic matter. Especially during summer time, the minimal oxygen demand for fish is not preserved (Claus and Konermann 2014). Improved predictive methods are needed to reduce future ecological and economical costs.

The flow behavior of high-concentrated fine sediment suspensions is non-Newtonian and highly dependent on the shear rate, the grain size and the volume solid content. As a consequence, in classical hydrodynamic numerical models the applied Reynolds equations for Newtonian flow behavior are not suitable to model the fluid mud dynamics.

In hydrodynamic numerical models for large-scale applications, e. g. coastal engineering, the interaction between turbulent flow behavior and fluid mud are considered in different ways. Within the framework of the European project MAST2-CT92-0013, a three-dimensional hydrodynamic free surface flow model was developed, including a sediment module to simulate cohesive sediment problems (Le Normant et al. 1993). The fluid mud dynamics were modeled by a depth-averaged approach, where fluid mud was represented by a constant high viscosity (Malcherek et al. 1996). This model was applied for the Loire

Estuary under combination of a fluid mud module, erosion and deposition and a vertical 1D bed consolidation module (Le Normant 2000).

Another numerical solution was developed by H. R. Wallingford (Crapper and Ali 1997). However, their two-dimensional model is not suitable for the simulation of fluid mud, since the rheological shear-thinning behavior of mud as a function of the shear rate and the solid content is not considered. Furthermore, in the Delft3D software package a module for the simulation of fluid mud has been integrated by Winterwerp (2002). This module describes a depth-averaged fluid mud layer which is decoupled with the fluid layer above. The interaction of both layers is described by the interfacial shear stress. van Kessel et al. (2011) extended this approach by a dimensionless fluff layer exchange model which later was implemented into a three-dimensional model. Herein an additional layer was introduced where fine sediments were stored between the fluid and the mud layer. However, these models are not applicable for the simulation of the rheological behavior of fluid mud since they do not account for the rheology variation with solid content.

A new method was developed to simulate fluid mud dynamics in Knoch and Malcherek (2011) and Wehr (2012). The complex non-Newtonian behavior of fluid mud was simulated by an isopycnal numerical model. Within this approach, the fluid mud layer was discretized in layers of same bulk density, so-called isopycnals. The numerical solution of the isopycnal fluid mud layer is based on a three-dimensional hydrodynamic model in isopycnal coordinates (Casulli 1997). In this context, the shear-thinning flow behavior of fluid mud and the rheometric investigation of the yield stress were analyzed. Rheometrical measurements with different volume solid contents were performed so that for the first time a formulation was found for the rheological fluid mud viscosity, which accounts for the shear rate and the solid volume content simultaneously (Malcherek 2010; Malcherek and Cha 2011). However, within the isopycnal fluid mud approach the vertical interaction of individual layers under consideration of turbulence could not been realized.

In contrast to simulate mud dynamics by separating fluid mud and fluid layers, a continuous modeling approach was presented by Le Hir et al. (2000). Within this technique, water and soft sediment are regarded as a whole, so that vertical momentum diffusion is accounted for. The viscosity of the continuous phase was described in that case as the sum of the eddy viscosity and the rheological viscosity. The mud viscosity was parameterized according to a Bingham fluid, the computation of the eddy viscosity followed the mixing length concept. Nevertheless, Le Hir and Cayocca expanded their continuous model into 3D in order to simulate oceanic gravity flows (Le Hir and Cayocca 2002).

Another continuous approach to simulate the dynamics of fluid mud was developed by Roland et al. (2012): The so-called FLMUD module is based on Cartesian coordinates. The module was validated qualitatively by numerical experiments. However, a detailed validation and application to an estuary are still needed.

The application of a two-equation turbulence model was investigated by Toorman (2002) for concentrated suspension flows. He presented modifications within the classical $k$-$\varepsilon$-turbulence model while fluid mud is apparent. With increasing suspended solid concentrations towards the bottom, the flow is regarded to become more and more laminar, turbulence is destructed. The damping of turbulence was investigated in case of suspended solid concentrations and a reconstruction of the boundary conditions was explained as well as additional damping parameters were introduced. Modifications of the bottom boundary conditions were mentioned to be valid only for low concentrated suspensions, since for higher concentrations and laminar flow the shear stress velocity is overestimated. This was corrected by the introduction of additional empirical damping functions (Toorman 2002). Summing up, the $k$-$\varepsilon$-turbulence model is not applicable for fluid mud dynamics. As the lutocline and the fluid mud region are characterized by laminar flow conditions ($k = 0$), the $k$-$\varepsilon$-model will always be unstable in that case, since there is no laminar flow solution for $\varepsilon$. In order to apply a two-equation turbulence model within the continuous modelling approach a turbulence model is needed which guarantees numerical stability in laminar flow conditions. This can be achieved with the $k$-$\omega$-turbulence model.

The objective of this paper is to present a numerical modeling concept which is called the advanced continuous modeling approach. The concept is presented by means of a continuous vertical 1D model including a $k$-$\omega$-turbulence model and fluid mud rheology of the Ems Estuary. The model is applicable for turbulent flow in low concentrated suspensions as well as for laminar flow in high concentrated suspensions. The formation of river bed and a fluid mud layer is shown by applying the continuous modeling approach where turbulence is automatically turned off and rheological behavior becomes dominant. The turbulent eddy viscosity and the rheological viscosity are combined into an effective viscosity. The rheological viscosity, which was parameterized for Ems and Weser muds by Malcherek and Cha (2011) was implemented to account for the complex variations of the rheological viscosity. The computation of turbulence follows a $k$-$\omega$-turbulence model, which was adopted to model also zero turbulence inside high concentrated mud. Additionally, the distribution of sediments is calculated by the transport equation for suspended solids.

The results of this modeling method are presented and improvements are discussed for future modeling techniques.

## 2 Methodology

During the transport of suspended cohesive sediments, a density driven stratification of the vertical water column occurs. Different layers can be defined over the water depth, such as the low concentrated suspension layer, the high concentrated suspension layer, and the fluid mud layer.

Knowing that velocity fluctuations can have relevant influence on the settling resistance of a particle, the turbulent effects in granular suspensions have to be investigated. Since turbulent velocity fluctuations interact with sediment particles within the flow, an overall decrease of turbulence with increasing density can be observed and leads to a laminarization of the flow (Malcherek and Cha 2011). In comparison to low concentrated suspensions which are driven by turbulent effects, the laminar flow of the fluid mud layer depends on its rheological properties. A query-based distinction between turbulent and laminar flow regimes should be prevented, since the vertical stratification and the height of the fluid mud layer changes during different flow situations, as recent field measurements of Becker et al. (2018) showed. This leads to the argument that in a numerical model the transition from turbulent to rheological flow cannot be predicted in advance; it has to be a result of the numerical model itself. Therefore, it is necessary to investigate the continuous modeling approach for future modeling of fluid mud dynamics. Within this approach, the suspension is regarded as a continuum, where particle-particle interaction like flocculation and hindered settling are considered by empirical functions.

Furthermore, this concept is characterized by a continuous transition between the water and the solid phase. Sharp changes of the modeling regime will be prevented, as it would have been the case for query-based fluid mud models.

In order to couple flow dynamics of Newtonian and non-Newtonian behavior, the viscosity in the momentum equations is regarded as an effective viscosity $\nu_{eff}$, namely the ratio of the shear stress to shear rate. This effective viscosity is equivalent to the turbulent viscosity $\nu_t$ for the water column when there is no suspended matter present. With increasing suspended matter concentration, turbulence is damped and rheological flow behavior becomes more important so that $\nu_{eff}$ turns into the rheological viscosity $\nu_{rh}$, see Figure 1.

Using the effective viscosity as the only material parameter the three-dimensional momentum balance is written as:

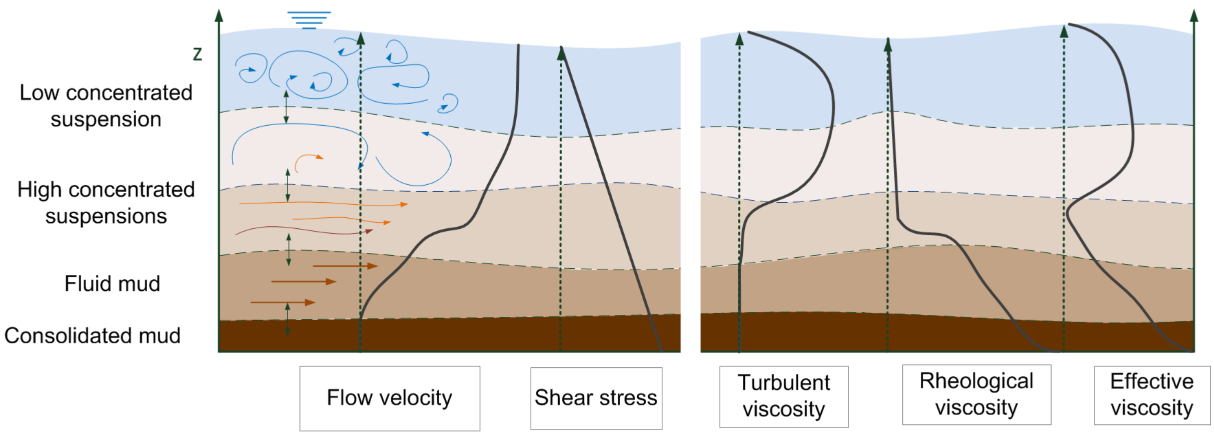


Figure 1: The schematic vertical profiles of the turbulent, rheological and effective viscosity and the resulting velocity profile are shown over total water depth, including the consolidated bottom and fluid mud.

$$\frac{\partial u_i}{\partial t} + u_j \frac{\partial u_i}{\partial x_j} = -\frac{1}{\rho}\frac{\partial p}{\partial x_i} + \frac{\partial}{\partial x_j}\left(\nu_{eff}\frac{\partial u_i}{\partial x_j}\right) + f_i, \tag{1}$$

with $u$ and $p$ being time averaged quantities for the flow velocity and pressure and $f_i$ describing the influence of external forces.

The advanced continuous modeling concept which is presented in this paper consists of the following main characteristics:

1. Mud rheology as a function of the solid content.
2. Modified $k$-$\omega$-turbulence model for stable laminar flow solutions.
3. Introduction of the effective viscosity as a transitional function from turbulent to rheological flow and vice versa.
4. Hindered settling within the sediment transport equation.

The numerical implementation of the mentioned aspects is described in the following sections.

## 2.1 Rheological properties of fluid mud in the Ems Estuary

Fluid mud is characterized as an aqueous mixture of clay and silt particles combined with organic matter. Mud samples show bulk densities of $\rho_b$ = 1080–1200 kg/m³ with corresponding bulk solid concentrations $c_b$ = 10–250 g/l (McAnally et al. 2007). Papenmeier et al. (2012) distinguished low-viscosity (20–200 g/l) and high-viscosity (200–500 g/l) muds. In literature different typical mean particle diameters were measured for fluid mud, reaching from 4.3 $\mu$m to $>$10 $\mu$m (Mitchell and West 2002; Wells and Coleman 1981). Fluid mud samples from the lower Ems show particle size distributions in the same range with $d_m$ = 10–20 $\mu$m, see Figure 2.

Fluid mud behaves as a viscoplastic fluid with a true yield stress. Its flow behavior is characterized by a non-linear increase of the shear stress for low-deformation rates and Bingham flow behavior for higher shear rates (Toorman 1995). The viscosity decreases with increasing shear rates thus fluid mud is a shear thinning fluid (Malcherek and Cha 2011). Shear thinning behavior in fluid mud can be explained by flocculation and floc break-up processes induced by organic material (Faas and Wartel 2006).

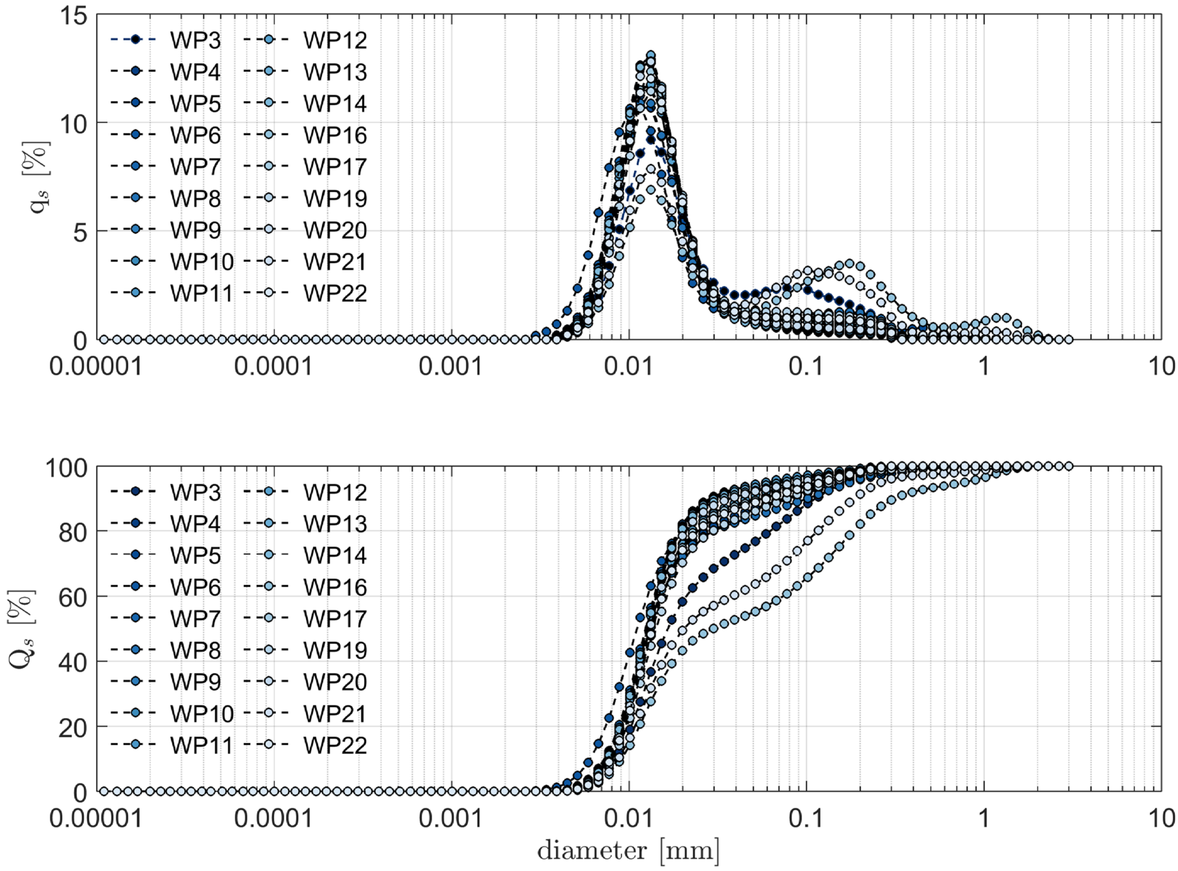


Figure 2: The particle size distribution is shown as a frequency distribution (upper figure) and as cumulative grading curves (lower figure) of fluid mud samples from the lower Ems between Leerort (WP3) and Weener (WP22). They were measured with a Horiba Particle Sizer. The evaluation results in a median particle diameter 10 $\mu$m< $d_m$ < 20 $\mu$m. According to the Wentworth scale, the sample can be described as fine silt (Wentworth 1922).

It is suggested in the Bingham model that mud has a Newtonian flow behavior when exceeding the critical yield stress $\tau_y$ (Coussot 1997). In fact, rheometrical measurements do not show such behavior, e.g. Malcherek (2010). The Worrall-Tuliani model which is based on structural kinetics theory describes the low shear rate region in an additional term, and includes formulations for flocculation and floc break-up (Worrall and Tuliani

1964). The Worrall-Tuliani model was extended by Malcherek and Cha for the dependency on the volumetric solid content $\phi$ (Malcherek 2010):

$$\tau(\dot{\gamma}, \phi) = \tau_y(\phi) + \mu_\infty(\phi)\dot{\gamma} + \frac{c_{floc}(\phi)\Delta\mu(\phi)\dot{\gamma}}{c_{break}\dot{\gamma} + c_{floc}(\phi)}, \quad (2)$$

where $\tau_y$ is the yield stress, $\mu_\infty$ is the appearing viscosity when all floc bonding is destroyed, $\dot{\gamma}$ is the shear rate, $\Delta\mu$ is the appearing viscosity when all floc bonding is intact and $c_{floc}$ and $c_{break}$ are parameters for growth and destruction of flocs. Here, floc growth has to be understood as shear induced growing of flocs. In this context shearing can also be responsible for the opposite, namely floc destruction. Both processes occur simultaneously, as documented in Spicer and Pratsinis (1996).

Within the MudSim project, fluid mud samples were analyzed from the Ems and Weser estuaries due to their rheological behavior. The mud samples were prepared for different solid contents $\phi$ and measured with an Anton Paar rotational rheometer. Different rheological models were applied for parameter estimation. Here we present the application of an extended Worall-Tuliani model. According to Eq. (2), five parameters had to be approximated in dependency of $\phi$: $\tau_y$, $\mu_\infty$, $\Delta u$, $c_{floc}$ and $c_{break}$.

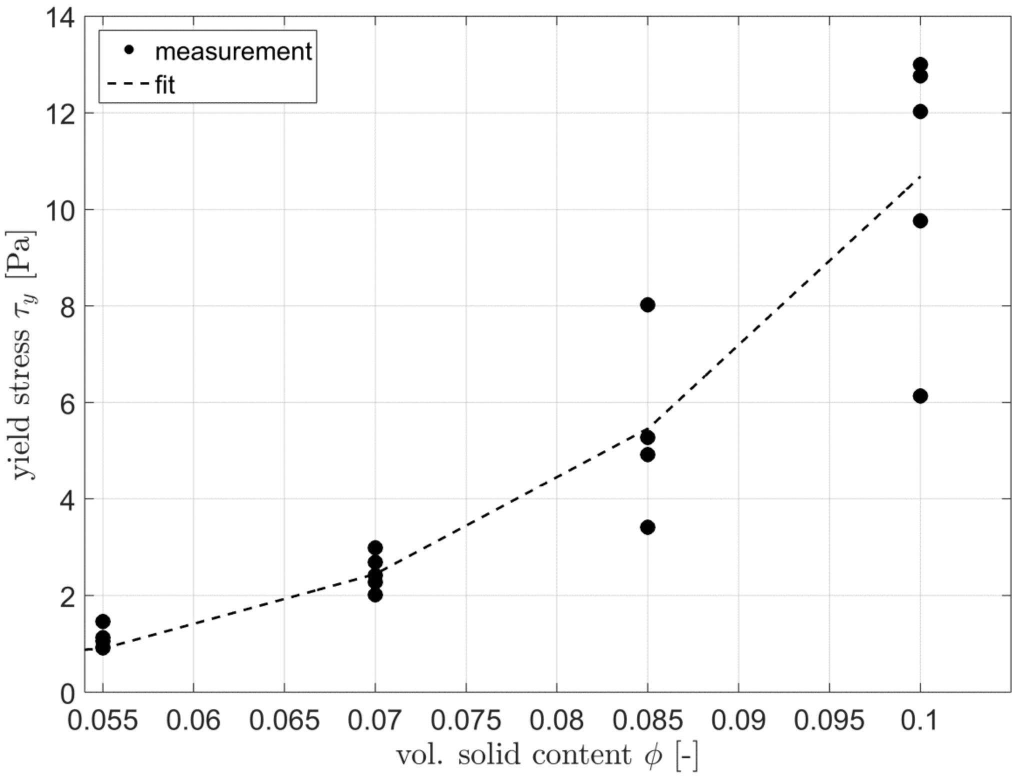


Figure 3: Performed yield stress measurements during the project MudSim for different solid contents $\phi$ = 0.055, 0.07, 0.085, 0.1 and a corresponding fitting curve which applies the Bingham relation between yield stress and solid content (modified after (Malcherek and Cha 2011). Measurements were conducted in CSS mode and plate-plate configuration under a constant temperature $T$= 20°C.

First, the relation between the yield stress $\tau_y$ and $\phi$ was investigated. Figure 3 shows the results of the rheometrical yield stress measurements. Samples with four different volume solid contents ($\phi$ = 0.055, 0.07, 0.085, 0.1) were investigated in CSS (controlled shear stress) mode and plate-plate configuration to detect the initiation of movement. A constant temperature of $T$ = 20°C was set during the measurements, see Malcherek (2010) for more details of the conducted measurements. The yield stress increases non-linearly with solid content. Similar behavior is presented in Kotzé et al. (2015) for the relation of yield stress and solid content for waste water sludge. Here the scattering of the measured data can be explained by variations in the grain and floc composition of single samples.

For numerical simulations the yield stress was fitted using the formulation:

$$\tau_y = \tau_{y0}\phi^n \tag{3}$$

The fitting parameters $\tau_{y0}$ = 6980 Pa and $n$ = 3.638 verified the data obtained by Migniot (1968), stating that $n$ is close to 4.

In case of very high shear rates, it can be assumed that all floc bondings are destroyed, the resulting viscosity is described by $\mu_\infty$. Further it is assumed that in case of $\phi$ = 0, $\mu_\infty$ should be equal to the dynamic viscosity of water $\mu_0$ = 0.001 Pa s. This leads to following formulation (Eq. 4):

$$\mu_\infty = \mu_0 \exp(a_1\phi), \tag{4}$$

with $a_1$ = 20.92. The viscosity $\Delta\mu$ for intact floc bondings was parameterized by following a linear relation, where $b_2$ = 8.439 Pa·s (Eq. 5).

$$\Delta\mu = b_2\phi \tag{5}$$

Finally, the process of floc growth $c_{floc}$ is expected to be a function of solid content as well, which is parametrized by $a_2$ = 88.1 Hz and $b_3$ = 1.403 (Eq. 6)

$$c_{floc} = a_2\phi^{b_3}, \tag{6}$$

and $c_{break}$ = 0.2619 is describing the destruction of flocs due to shearing. Eq. 3–Eq. 6 were included in Eq. (2) in order to obtain the necessary parameters via surface fitting (Malcherek 2010).

For the implementation of the rheological viscosity into the continuous modeling approach the kinematic rheological viscosity is calculated as

$$\nu_{rh} = \frac{\mu_{rh}}{\rho_b} = \frac{1}{\rho_b}\left(\frac{\tau_y}{\dot{\gamma}} + \mu_0 \exp(a_1\phi) + \frac{c_{floc}\Delta\mu}{c_{break}\dot{\gamma} + c_{floc}}\right). \tag{7}$$

As this parametrization shows, the rheological model depends on the solid volume content, among others. As a consequence, the rheological model covers the entire water column from fluid mud and high concentrated suspensions to low concentrated suspensions, e. g. in case of low or zero concentrations, the yield stress decreases and the rheological viscosity is reduced to the dynamic viscosity $\mu_0$ of water. Therefore, we claim that this approach can be applied to fluid mud as well as to clear water when turbulence is considered adequately. Hence, the rheological model is able to represent Newtonian fluids as well as non-Newtonian fluids.

 https://doi.org/10.18171/1.089101

## 2.2 The turbulence model

Within this work the $k$-$\omega$-turbulence model (Wilcox 1994) is applied for a continuous stratified suspension in a homogeneous boundary layer approach. The fundamental equations read:

$$\frac{\partial k}{\partial t} + u_j \frac{\partial k}{\partial x_j} = \frac{\partial}{\partial x_j}\left( (\nu_{rh} + \nu_t \sigma_*) \frac{\partial k}{\partial x_j} \right) + P_k + G - \beta^* k\omega \tag{8}$$

$$\frac{\partial \omega}{\partial t} + u_j \frac{\partial \omega}{\partial x_j} = \frac{\partial}{\partial x_j}\left( (\nu_{rh} + \nu_t \sigma_\omega) \frac{\partial \omega}{\partial x_j} \right) + \alpha \frac{\omega}{k} P_k - \beta \omega^2 \tag{9}$$

The turbulence model includes the creation of turbulence due to shear $P_k = \nu_t \left(\frac{\partial u}{\partial z}\right)^2$, transport of turbulent kinetic energy $k$, turbulence damping $G$ due to density stratification and $\omega$ as the dissipation rate of turbulent kinetic energy. Classical constants are applied in the $k$-$\omega$-model, $\gamma^* = 1$, $\alpha = 5/9$, $\beta^* = 0.09$, $\beta = 3/40$, $\sigma_* = 0.5$ and $\sigma_\omega = 0.5$ (Wilcox 1994). Stable stratification is assumed, so that the buoyancy term is not considered for the scale where dissipation occurs (Uittenbogaard et al. 1992). $G$ describes the destruction of turbulence due to stratification effects (Eq. 10), with $Sc$ as the turbulent Schmidt number (Violet 1988). Here, stratification occurs due to density gradients, with $\rho_b$ as the bulk density of the suspension.

$$G = \frac{g}{\rho_b} \frac{\nu_t}{Sc} \frac{\partial \rho_b}{\partial z} \tag{10}$$

The turbulent viscosity is calculated by means of the turbulent kinetic energy $k$ and the dissipation rate $\omega$ (Eq. 11).

$$\nu_t = \gamma^* \frac{k}{\omega} \tag{11}$$

In contrast to the $k$-$\varepsilon$-turbulence model, for instance, the $k$-$\omega$-turbulence model is applicable for low-Reynolds flows and for modeling the viscous sublayer without introducing additional damping functions. Within the viscous sublayer the condition $k = 0$ has to be full filled, which does not produce numerical instabilities in the $\omega$-equation. The transport equation for $\omega$ can be rewritten by simple mathematical substitution of $P_k$ and $\nu_t$, according to:

$$\frac{\partial \omega}{\partial t} = \frac{\partial}{\partial x_j}\left( (\nu_{rh} + \nu_t \sigma_\omega) \frac{\partial \omega}{\partial x_j} \right) + \alpha_\omega \gamma^* \omega^2 \left( \frac{\frac{\partial u}{\partial z}}{\omega} \right)^2 - \beta \omega^2 \tag{12}$$

With that form it is evident that the $\omega$-equation is being decoupled of the $k$-equation. Therefore the $k$-$\omega$ model is able to provide a stable solution for laminar flow, even when the turbulent kinetic energy is zero.

The bottom boundary conditions are set to $k_b = 0$ and $\omega_b = S_r \frac{u_*^2}{\nu_0}$, with $u_* = \sqrt{gJh}$ being an estimate of the shear stress velocity, $J$ the slope of the bed, $S_r = \frac{2500}{(k_s^+)^2}$, $k_s^+ = \frac{u_* k_s}{\nu_0}$ and $k_s = 3\ d_m$. This boundary condition is applied at the bottom boundary of the numerical model which could be below a fluid mud layer. The turbulent kinetic energy at the surface boundary is described by a homogeneous Neumann condition, whereas a Dirichlet boundary condition is assumed for $\omega$ at the free surface.

In order to extend the $k$-$\omega$-model to the whole simulation domain, i.e. also into a fluid mud bottom, the behavior in mud has to be analyzed: When a high concentration mud is formed and the flow does not exceed the yield stress, the shear rate is zero and turbulence production $P_k$ is also zero: The $k$-$\omega$ as well as the $k$-$\epsilon$-model do not predict any turbulence which is absolutely correct. However, the $k$-$\epsilon$-turbulence model was originally developed for fully turbulent conditions and it is not valid for low-Reynolds flows or the viscous layer near the immobile bed. This behavior of the $k$-$\epsilon$-model is controlled by the bottom boundary condition $\epsilon_b = \frac{u_*^3}{\kappa z_0}$, where $z_0$ describes the modeling boundary and $\kappa = 0.41$ the Kármán constant. The application of the turbulence model for a continuous phase, including immobile conditions, makes a model necessary which is able to overcome the disadvantage of the $k$-$\epsilon$-model.

The advantage of the $k$-$\omega$-turbulence model is the ability to consider the Stokes' wall condition ($u_b$ = 0, $k_b$ = 0) in the bottom boundary conditions for $\omega$. Doing so, the $k$-$\omega$-model is able to resolve the viscous layer near the immobile bed. In case of an immobile bed, i.e. no shear rate and no turbulence production at the bed, $\omega$ will be constant and equal to its lower boundary value $\omega_b$.

Hence, the $k$-$\omega$-model is capable to reproduce the transient behavior from laminar to turbulent flows. Here the turbulent kinetic energy is zero and therefore $\nu_t$ is zero. In this case the viscosity reduces to its laminar value. There remains the question what is $\omega$ in that case. Since the introduction of the $k$-$\omega$-model there is a discussion, what $\omega$ really represents. Because it has a finite value at closed boundaries where the turbulent kinetic energy is zero, it cannot be interpreted as a dissipation rate. Within this modeling concept $\omega$ is rather the potential of a dissipation rate. It describes the ability of turbulence destruction due to the solid content and not the actually destroyed turbulent energy.

The modeling approach presented here does not need the distinction of mud and water column by a lutocline anymore. Therefore, we do not need artificial boundary conditions at this artificial boundary any more. Here a lot of work was done in the past: Toorman for example proposed to include the destructive term into the bottom boundary conditions of the $k$-$\epsilon$ turbulence model, which was done by the flux Richardson number $Ri_f$ (Toorman 2002). This procedure prevents the bottom boundary condition from being set to zero for turbulent kinetic energy, which has to be the case in fluid mud. Setting $k = 0$ at the bottom, would have provided an unstable numerical scheme, since the dissipation equation includes division by $k$. Additionally, while reducing the bottom boundary conditions, empirical reduction parameters for the turbulence production term $P_k$ would have been needed to prevent the model from producing turbulence inside the mud layer. Therefore, such an approach is only valid when a pronounced lutocline is formed. In reality, all kinds of concentration distributions can occur. This can only be described by a continuous modeling approach in combination with a suitable turbulence model. This new development of the continuous approach is proposed in this paper.

## 2.3 The effective viscosity

The turbulent viscosity has to become zero in a resting mud bottom on the one hand, and on the other hand, the rheological viscosity has to vanish if no suspended matter is present.

Therefore, we assume the effective viscosity to be the sum of both parts (Figure 1), i.e. the turbulent eddy viscosity $\nu_t$ and the rheological viscosity $\nu_{rh}$.

$$\nu_{eff} = \nu_t + \nu_{rh} \tag{13}$$

It has to be mentioned that both viscosities have different physical meanings. As an increase of turbulent viscosity is interpreted as an increase of turbulence, the rheological viscosity is the opposite. An increase of rheological viscosity goes with an increase of the solid content and therefore with a decrease of turbulence. In a resting sediment bottom the turbulent kinetic energy is zero and therefore the turbulent viscosity also vanishes. On the other hand, in a clear water column the rheological viscosity transforms into the molecular viscosity of water.

## 2.4 Transport equation

The transport of suspended material is described by the time averaged transport equation for suspended solids, including the concentration flux $\Phi_c = u_{i,s}c - K_t\,\mathrm{grad}(c)$, where $K_t$ is the eddy diffusivity (Malcherek 2016).

$$\frac{\partial c}{\partial t} + \mathrm{div}\big(u_i c - K_t\,\mathrm{grad}(c)\big) + \frac{\partial w_s c}{\partial z} = 0 \tag{14}$$

where $w_s$ is the particle settling velocity. $K_t$ is expressed by the turbulent Schmidt number $Sc = \frac{\nu_t}{K_t}$. It is shown in Absi et al. (2011) that $Sc \approx 1$ for turbulent diffusion of small particles. Both, the boundary conditions at the water surface and at the bottom are implemented as zero-flux Neumann conditions.

As it is elaborated in Whitehouse et al. (2000), the settling velocity $w_s$ is difficult to approximate since it depends on a variety of different parameters like density variations, flocculation ability, salinity and hindered settling amongst others. Furthermore, the settling velocity for cohesive sediments is always site-specific. A common approach is based on the equilibrium of gravitational and drag forces, which results in the Stokes' formula (Eq. 15) for stationary settling of a single particle, with $d$ being the particle diameter, $\mu$ being the dynamic viscosity of the surrounding fluid, $g$ the gravity acceleration and $\rho_s$, $\rho_f$ the solid and fluid density, respectively (Malcherek 2016).

$$w_{s,0} = -\frac{(\rho_s - \rho_f)gd^2}{18\mu} \tag{15}$$

Takács et al. (1991) divide the settling of particles into four regimes defined by their concentration: (i) discrete particle settling, (ii) flocculent particle settling, (iii) hindered settling, and (iv) compression settling. The hindered settling regime begins at concentrations greater than 2 g/l, according to them. Furthermore, Winterwerp (2002) explains that hindered settling occurs until the gelling concentration $c_{gel}$ of mud is reached. For three evaluated experimental data sets, he identifies the gelling concentration between 40 g/l and 120 g/l.

In the present model the effect of hindered settling is taken into account by a concentration dependent reduction of Stokes' settling velocity:

$$w_{s,HS} = \frac{1}{2}\, w_{s,0}\left(1 - \tanh\left(\gamma_1\left(\frac{c}{c_{gel}} - 1\right) + \gamma_2\right)\right). \quad (16)$$

The parameters $\gamma_1$ and $\gamma_2$ are shape parameters, describing the sharpness and the horizontal translation of the function. Both parameters depend on the type of sediment.

In literature several approaches exist to account for hindered settling. Figure 4 gives a graphical comparison of the dimensionless settling velocities computed by the approaches of Richardson and Zaki (1954), Takács et al. (1991), van Rijn (1993), Winterwerp (2002) and Eq. 16. Since the approach of Winterwerp was evaluated for the Ems estuary, it is regarded as reference. Therefore the parameters were set to $c_{gel}$ = 100 g/l, $\gamma_1$ = 4.8 and $\gamma_2$ = 2.7.

This settling velocity approach does not take into account flocculation because $w_{s,0}$ is calculated according to the classical Stokes' formulation. However this approach could also be valid to describe flocculation when settling velocity formulations are applied including floc dynamics. Here, for example, the approach of Dyer and Manning (1999) could be used, who describe a settling velocity formulation based on fractal floc dimensions, which is applicable for flocculation processes.

The hyperbolic tangent function is well suited for the description of the settling velocity. The parameters of this function can easily be adopted to experimental data sets for hindered settling.

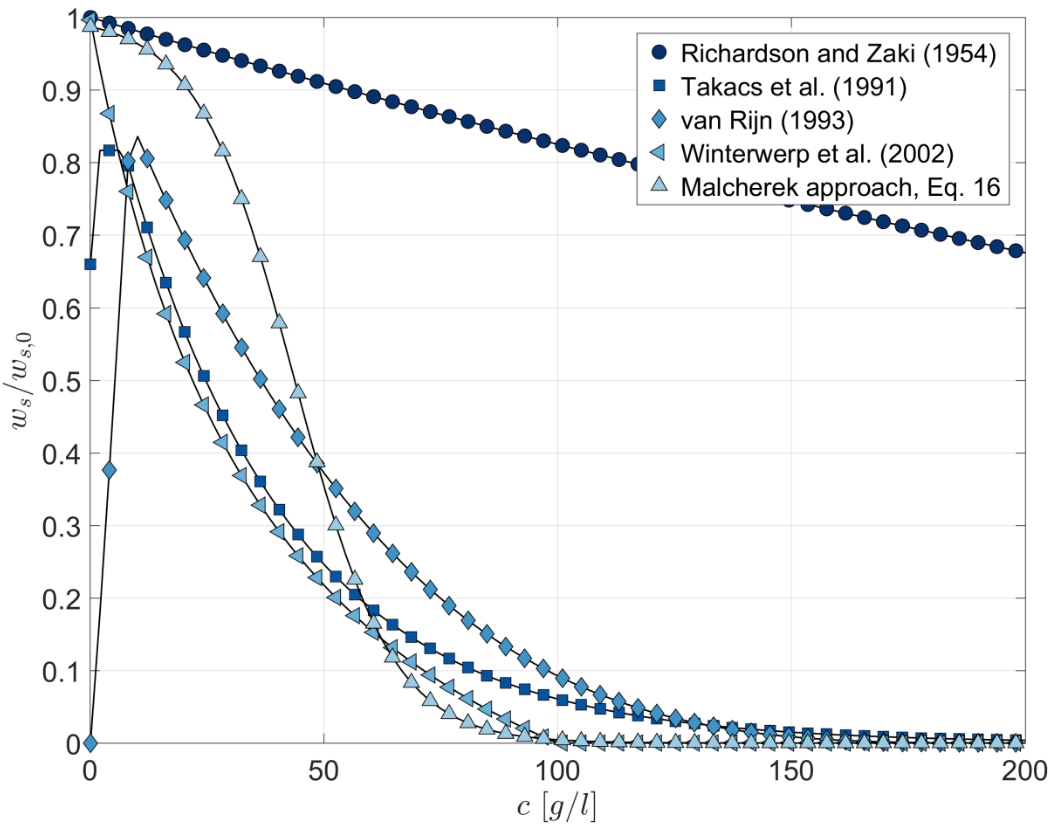


Figure 4: comparison of different hindered settling approaches to calculate the settling velocity of sediments for $c_{gel}$= 100 g/l and $d_m$= 20 $\mu$m.

## 2.5 Description of the numerical model

In order to investigate the continuous transition of the processes in vertical direction, the three-dimensional estuarine system is reduced to a vertical one-dimensional turbulent boundary layer flow. To describe the formation of fluid mud, the momentum equation including the effective viscosity $\nu_{eff}$ (Eq. 13) is coupled with the transport equation (Eq. 14) and the turbulence model.

For homogeneous boundary layer problems in an open channel, Eq. (1) can be rewritten as

$$\frac{\partial u}{\partial t} = \frac{\partial}{\partial z}\left(\nu_{eff}\frac{\partial u}{\partial z}\right) + Jg \tag{17}$$

with $\frac{\partial u}{\partial t}$ describing the unsteady evolution of the mean flow velocity in x-direction over depth (z-direction) and $Jg$ accounting for external forces due to the bed slope $J$. The velocity boundary condition at the bottom reads a no-slip condition, $u_b = 0$, whereas the surface boundary is described by a homogeneous Neumann condition.

For a homogeneous boundary layer problem, the transport equation for mean concentration $c$ is written as:

$$\frac{\partial c}{\partial t} = \frac{\partial}{\partial z}\left(K_t\frac{\partial c}{\partial z}\right) - \frac{\partial w_s c}{\partial z}, \tag{18}$$

while the $k$-$\omega$-model reads:

$$\frac{\partial k}{\partial t} = \frac{\partial}{\partial z}\left((\nu_{rh} + \nu_t\sigma_*)\frac{\partial k}{\partial z}\right) + P_k + G - \beta^* k\omega \tag{19}$$

$$\frac{\partial \omega}{\partial t} = \frac{\partial}{\partial z}\left((\nu_{rh} + \nu_t\sigma_\omega)\frac{\partial \omega}{\partial z}\right) + \alpha\frac{\omega}{k}P_k - \beta\omega^2 \tag{20}$$

Due to the rheological viscosity and the yield stress $\tau_y$, the model is able to simulate the bottom, even for bottom velocities $u = 0$. In that case, there is no vertical velocity gradient, so that turbulence production and the turbulent viscosity is also zero.

This approach allows to define $k_b = 0$, as the bottom boundary condition for turbulent kinetic energy.

Inside high concentrated mud, turbulence is supposed to be destructed and is expected to reach very small values or even zero. In turn, the potential of the dissipation should be constantly high inside the mud.

In addition with the implemented rheological viscosity, the model is able to switch automatically between no-flow, rheological flow and turbulent flow.

# 3 Results of the 1DV model

Before showing the qualitative behavior of fluid mud formation, modeling results are compared with results of existing 1DV models in case of low and intermediate concentrations. Afterwards, the formation of a fluid mud layer and the retroactive effect on the velocity, the turbulent kinetic energy and the turbulent viscosity are described. Additionally, the resulting effective viscosity is presented.

The model is based on a semi-implicit finite differences Crank-Nicolson scheme with a grid resolution $\Delta z$ = 0.05 m and a time step $\Delta t$ = 0.05 s.

### 3.1 Comparison to related studies

As one of the results of the COSINUS-project within the MAST3 research programme, Winterwerp et al. (2002) presented a 1DV model to study the behavior of concentrated benthic suspension flows. Turbulence was modeled by the $k$-$\epsilon$ turbulence model, including Munk-Anderson damping functions to consider stratification effects. In this study, the rheological viscosity was not considered. Such simplification is reasonable for low concentrations but not for high concentrated flows any more. Modeling results were presented for $c_0$ = 37 mg/l as homogeneously distributed initial concentration and for different shear stress velocities. Furthermore, constant water depth $h$ = 16 m and constant settling velocity $w_s$ = –0.5 mm/s were assumed. Figure 5 describes vertical steady state concentration profiles for mentioned settings. On the left hand side the results of the modeling approach presented here and on the right hand side) the COSINUS results are shown.

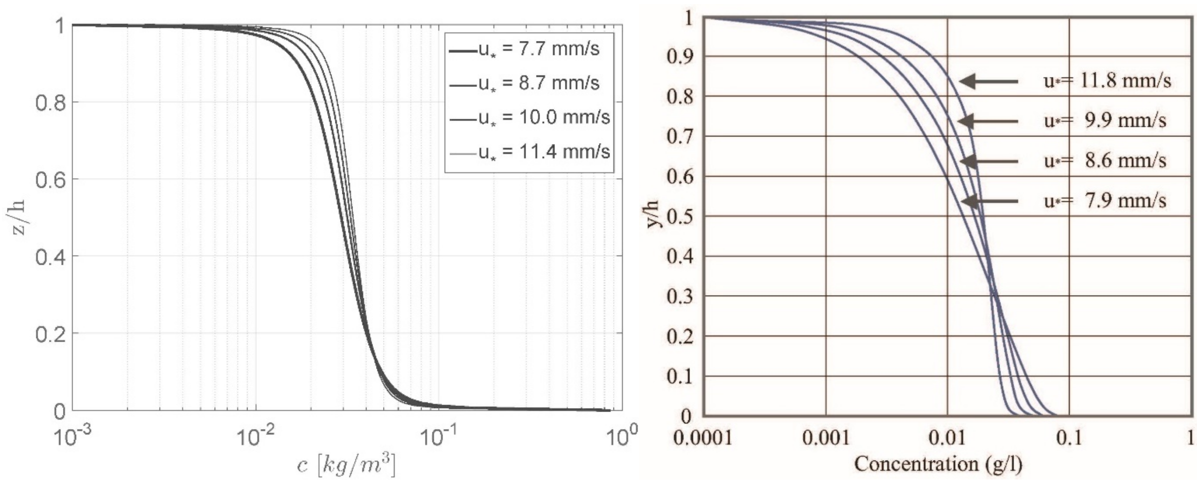


Figure 5: Comparison of the (left) simulated concentration profiles with (right) earlier results of Winterwerp et al. (2002) for low concentrations. The settings were kept similar: $h$ = 16 m, constant $w_s$ = -0.5 mm/s, $c_0$ = 37 mg/l and varying shear velocities. Here, $u_*$ = 11.4 mm/s, 10.0 mm/s, 8.7 mm/s and 7.7 mm/s are chosen.

The shape of the concentration profiles depends on the shear velocity $u_*$. With increasing shear velocity turbulence increases, which counteracts the settling of particles. The concentration profiles are regarded to be qualitatively comparable for both 1DV models, however within the COSINUS results particles tend to settle quicker. This behavior is explained when observing the modeled turbulent viscosity profiles, shown in Figure 6 (left). Additionally, the analytical solution $\nu_t = \kappa u_* z\left(1 - \frac{z}{h}\right)$ is given. Differences between the analytical and the numerical solutions are due to the turbulence damping term (Eq. 10), which reduces the turbulent kinetic energy when density gradients occur. While regarding maximum dimensionless values for turbulent viscosity in the range $\nu_t^+$ = 0.07 – 0.078, the COSINUS model predicts values in the range $\nu_t^+$ = 0.017 – 0.048. The differences are due to the added Munk-Anderson damping functions within the COSINUS model. However, greater turbulence is responsible for the steeper concentration profiles in comparison to the results of Winterwerp et al. (2002).

While describing the continuous transition from turbulent to rheological flow, the rheological viscosity must be regarded in case of low concentrations. Figure 6 (right) presents the corresponding vertical profiles of the dimensionless rheological viscosity $\nu_{rh}^{+}$. Since the particle concentration is low in this case, the rheological viscosity is low, as well. It can be seen that the rheological viscosity has minor influence in comparison to the turbulent viscosity. This will change when higher concentrations are considered.

It was shown, that the modeling approach presented here can be applied for low concentrations providing comparable results to earlier studies without changing any model parameters. At low concentrations, the influence of $\nu_{rh}$ is low, as well and the flow is modeled to be fully turbulent; at high concentrations only the rheological viscosity is taken into account.

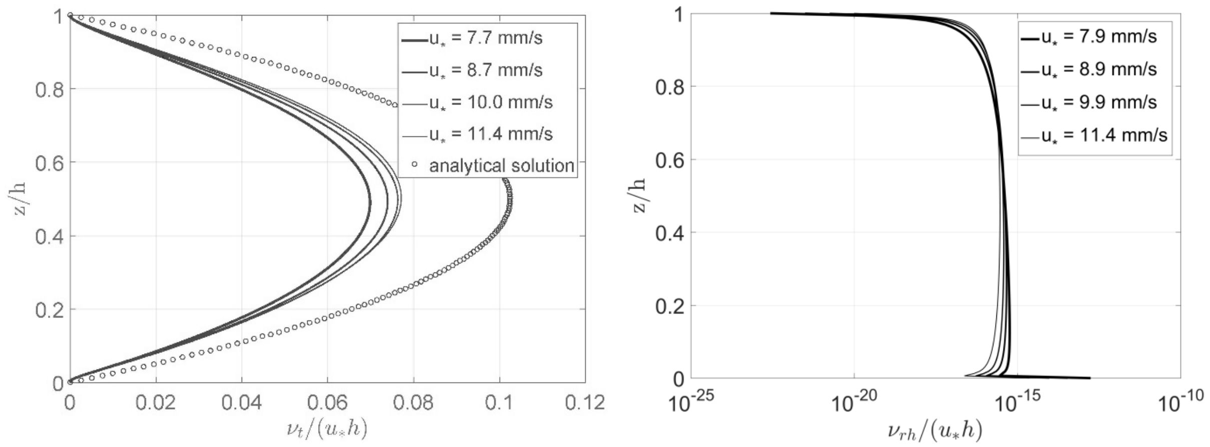


Figure 6: Comparison of the simulated dimensionless (left) turbulent and (right) rheological viscosity profiles. Additionally, the analytical solution is shown for the parabolic turbulent viscosity profile. Numerical settings were set to: $h$ = 16 m, constant $w_s$ = -0.5 mm/s, $c_0$ = 37 mg/l and varying shear velocities. Here, $u_*$ = 11.4 mm/s, 10.0 mm/s, 8.7 mm/s and 7.7 mm/s are chosen.

Le Hir and Cayocca presented another 1DV model, which is based on a continuous modeling approach (Le Hir and Cayocca 2002). They evaluated their model for initial concentrations $c_0$ = 0.1, 1, 10 and 30 g/l. The turbulence closure is achieved by a simple mixing-length approach, including the gradient Richardson number and empirical parameters to account for turbulence damping. Transport of turbulence was not taken into account. The so-called generalized viscosity was introduced, including the turbulent viscosity and the rheological viscosity according to Bingham's law.

Their model is based on a homogeneous initial concentration, a constant settling velocity $w_s$ = -1 mm/s, $h$ = 10 m and $u_*$ = 0.01 m/s, while the results represent the final stationary distribution.

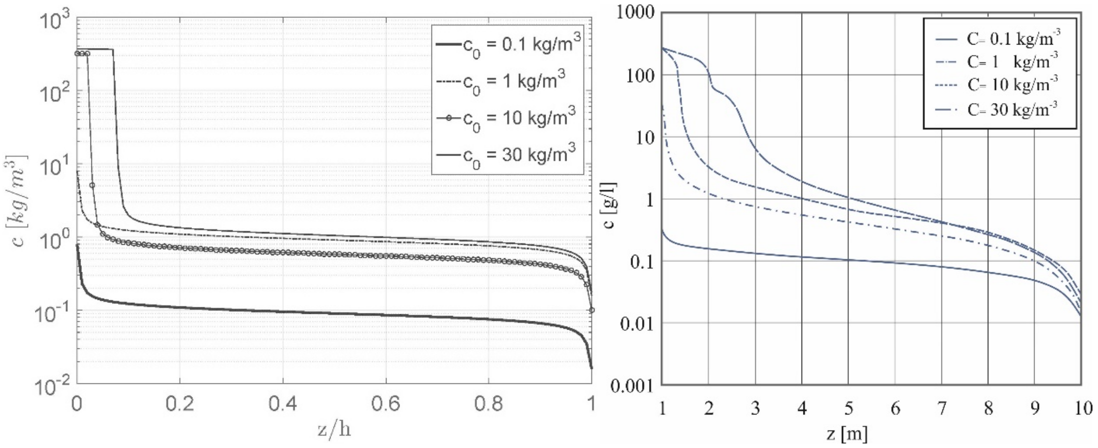


Figure 7: Comparison of the (left) simulated concentration profiles with (right) earlier results of Le Hir and Cayocca (2002) for initial concentrations $c_0$ = 0.1, 1, 10 and 30 g/l. Numerical settings were kept the same: $h$ = 10 m, constant $w_s$ = -1 mm/s and $u_*$ =0.01 m/s.

Figure 7 presents a comparison of vertical concentration profiles for both, the model of Le Hir and Cayocca and the new model presented in this paper. Initial concentrations $c_0$ = 0.1, 1, 10 and 30 g/l were chosen. The steady state concentration profiles show a comparable behavior, however differences in the shape are explained by differing turbulence, rheological and hindered settling models. Regarding the concentration profiles for $c_0$ = 10 g/l and 30 g/l in 7 (left), the creation of a concentrated mud layer can be observed.

Figure 8 presents the corresponding dimensionless turbulent and rheological viscosity profiles. The results for turbulent viscosity show the known parabolic shape, being zero at the bottom and the water surface. However, for $c_0$ = 10 g/l and 30 g/l turbulent viscosity becomes zero above the bottom at $z/h$ = 0.05 and $z/h$ = 0.1, respectively. In this layer no turbulence occurs, which means that there is laminar or no-flow at this position. The corresponding behavior for the rheological viscosity is shown in Figure 8 (right). An increase of rheological viscosity is visible below $z/h$ = 0.05 and $z/h$ = 0.1 for $c_0$ = 10 g/l and 30 g/l.

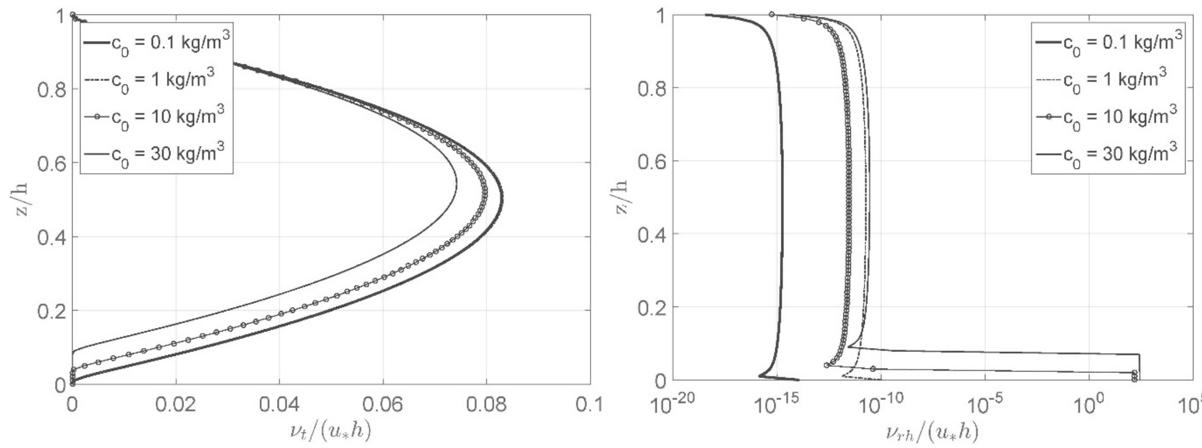


Figure 8: Steady-state solutions of the simulated dimensionless (left) turbulent and (right) rheological viscosity profiles for initial concentrations $c_0$ = 0.1, 1, 10 and 30 g/l concentrations. Numerical settings were set to: $h$ = 10 m, constant $w_s$ = -1 mm/s and $u_*$ = 0.01 m/s.

It is shown that this modeling approach is capable of simulating low and intermediate concentrated flows without changing parameters. Results of the new model are qualitatively comparable with the results of Le Hir and Cayocca (2002). The model automatically recognizes laminar and no-flow regimes, which can be seen in the velocity profiles. The creation of immobile bed and the corresponding velocity profiles are presented in section 3.2.

## 3.2 Application for high concentrations

In order to enforce the creation of a high concentrated bottom layer within the model, two possible strategies can be followed. (i) The initiation of a high concentrated bottom and a lower concentration above. (ii) The initiation of a homogeneously distributed high concentration over the entire water depth. The second was applied within this model, with an initial concentration $c_0$ = 30 g/l. The initial conditions for velocity, turbulent kinetic energy, dissipation rate and turbulent viscosity were set to zero.

Following parameters had been applied: $h$ = 10 m, as constant water depth, $J$ = 2·10$^{-5}$ and $z_0$ = 6.8·10$^{-5}$ m.

### 3.2.1 Formation of a concentrated mud layer

The formation of a fluid mud layer is shown in Figure 9 for different mean particle diameters, whereas the initial concentration is $c_0$ = 30 g/l. First, results are presented for vertical steady state velocity and concentration profiles. Velocity profiles were made dimensionless due to division by $u_*$. Different mean particle diameters $d_m$ = 15 $\mu$m, 30 $\mu$m, 63 $\mu$m were chosen to show the different settling behavior.

The creation of high concentrated mud ($c >$ 250 g/l) at the bottom is visualized by the sudden jump in the concentration profile. The fluid mud layer is indicated by the lutocline layer, which describes the region of rapid change in density or concentration gradient by depth (Dronkers and van Leussen 2012). Furthermore, the lutocline layer describes the transition of the mobile fluid mud to the stationary fluid mud layer. This transition is characterized by a steep velocity gradient and therefore high shear rates $\dot{\gamma} = \frac{\partial u}{\partial z}$. A smaller mean particle diameter results in lower settling velocities, therefore the concentration profile for $d_m$ = 63 $\mu$m presents the sharpest jump in the velocity and concentration profiles. In this case, there is no flow velocity at the bottom, whereas for $d_m$ = 15 $\mu$m and 30 $\mu$m it shows mobile mud layers. This corresponds to the concentration profiles, since the concentration profile for $d_m$ = 15 $\mu$m, for instance, is more distributed over depth and therefore a lower concentrated bottom is formed as it is the case for greater $d_m$. Zero movement of concentrated mud is explained by the yield stress $\tau_y$, which is a function of the solid content Eq. (3) and which is not exceeded by the shear stress $\tau = \rho g h J$.

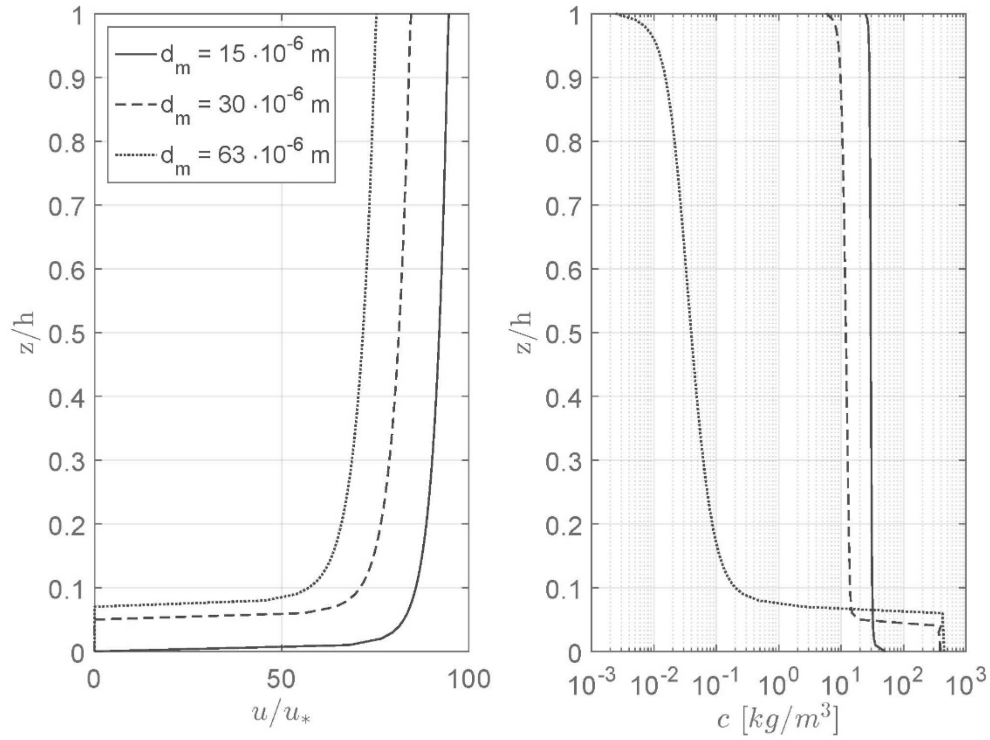


Figure 9: The numerical results of the vertical profiles for flow velocity and concentration are shown, while $h =$ 10 m, $J$ = 2·10$^{-5}$, $c_0$= 30 g/l and the mean particle diameter is varied ($d_m$ = 15 $\mu$m, 30 $\mu$m, 63 $\mu$m). The results are presented for steady state. Transitional behavior of no flow, rheological flow and turbulent flow is shown.

### 3.2.2 Turbulence production in mud

Furthermore, the simulated turbulent kinetic energy $k$ and the dissipation rate are shown for this scenario (Figure 10). Turbulence is zero when no flow is computed. The maximum of turbulent kinetic energy is always at the lutocline, since the shear rate reaches maximum values at the lutocline. Turbulence seems to be affected by the concentration. Greatest turbulent kinetic energy is observed for $d_m$ = 63 $\mu$m due to reduced water depth in case of bottom formation. The effect of turbulence damping due to stratified concentration profiles is shown within the profiles of turbulent viscosity in Figure 11 (left). Inside the mud layer turbulent kinetic energy is zero, which corresponds to immobile flow conditions shown in Figure 9 (left). This effect of laminarization emphasizes the significance of modeling fluid mud dynamics, since it has important effects on the flow velocity.

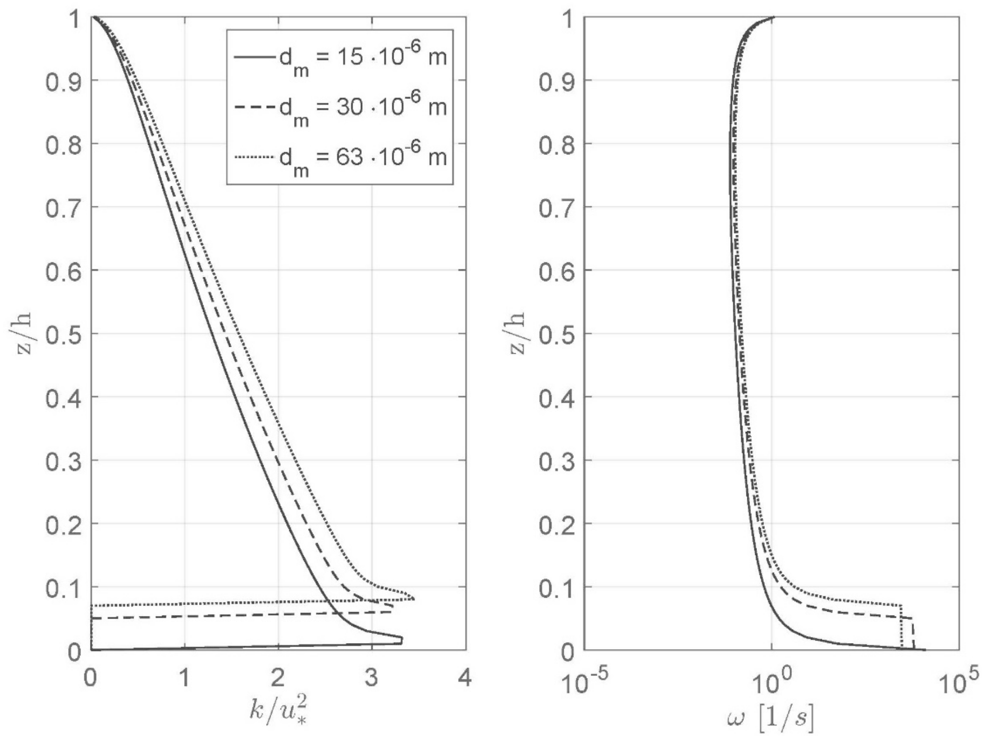


Figure 10: The numerical results of the vertical profiles for turbulent kinetic energy and the dissipation rate are shown, while $h$= 10 m, $J$= 2·10$^{-5}$, $c_0$= 30 g/l and the mean particle diameter is varied ($d_m$= 15 $\mu$m, 30 $\mu$m, 63 $\mu$m). The results are presented for steady state. Maximum values of turbulent kinetic energy appear at the lutocline, where the shear rate is the greatest.

Inside the immobile mud, where the turbulent kinetic energy is zero, no artificial turbulence is produced, which would lead to diffusion of the sediment. Likewise the dissipation rate is expected to be high over the entire depth of the immobile mud. Especially in case of $d_m$ = 63 $\mu$m this behavior is visible. Here, the created mud layer reaches until $z/h$ = 0.08, this can be recognized in constant high values for $\omega$.

As the greater particles ($d_m$ = 30 $\mu$m and 63 $\mu$m) settle faster towards the bottom and create a rigid bed, the finer particles ($d_m$ = 15 $\mu$m) are more distributed over the entire water depth. In this case the yield stress is exceeded by the acting shear stress and the suspension is flowing. Turbulence production reaches further downwards and acts as a diffusive mechanism, which hinders the particles from settling.

### 3.2.3 The turbulent and effective viscosity

The corresponding steady state viscosity profiles for $J = 2$ ·10$^{-5}$ (Figure 11) are presented. They are shown in dimensionless form through division by $h$ and $u_*$. It is shown that the turbulent viscosity automatically vanishes when the concentration is sufficiently high and that in turn, the rheological viscosity increases. The effective viscosity as the combination and transition of turbulent to rheological viscosity is described in semi-logarithmic scale. Further, the shear thinning behavior of fluid mud is visible, as the shear rate increases at the lutocline and at the bottom. This is shown for effective viscosity results of $d_m$ = 63 $\mu$m at $z/h$ = 0.07, $d_m$ = 30 $\mu$m at $z/h$ = 0.05, and $d_m$ = 15 $\mu$m at $z/h$ = 0.

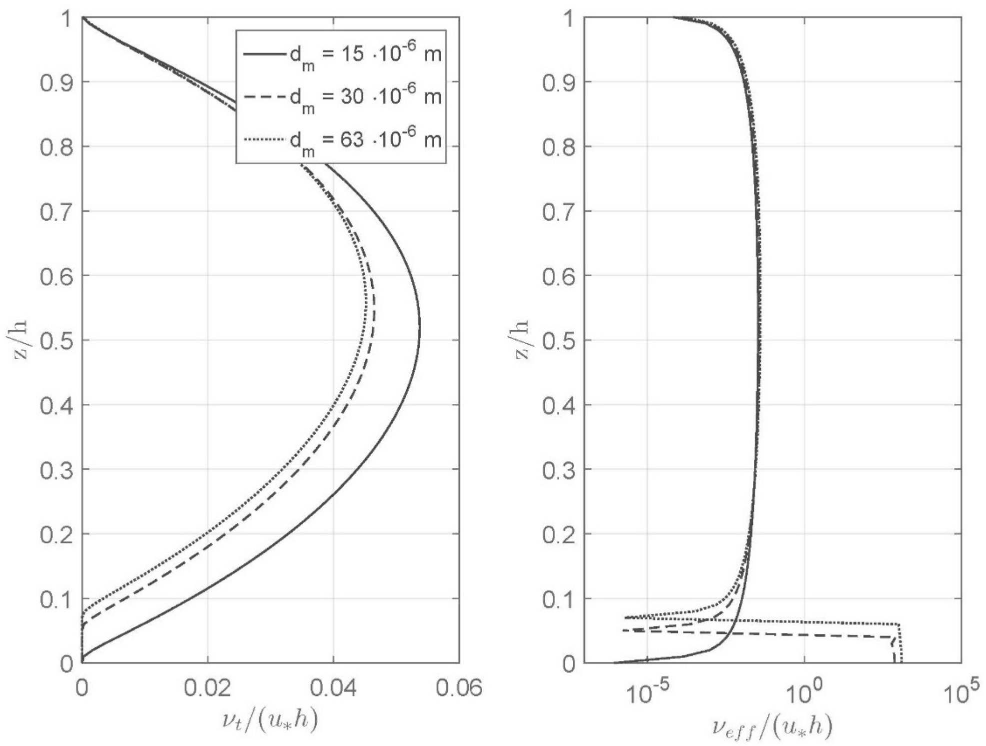


Figure 11: The numerical results of the vertical profiles for turbulent and effective viscosity are shown, while $h$= 10 m, $J$= 2·10$^{-5}$, $c_0$= 30 g/l and the mean particle diameter is varied ($d_m$ = 15 $\mu$m, 30 $\mu$m, 63 $\mu$m). The results are presented for steady state. Maximum values of turbulent viscosity appear at half of the flow depth and show parabolic profiles. The rheological behavior of the created mud is described by the effective viscosity.

In case of $d_m$ = 30 $\mu$m and $d_m$ = 63 $\mu$m, the profiles for turbulent viscosity (Figure 11) show a clear distinction between turbulent regime in the upper part and rheological regime in the lower part, beneath $z/h$ = 0.05 and $z/h$ = 0.07.The turbulent region is described by a parabolic distribution of $\nu_t$, maximum values are reached approximately in the middle of the turbulent region.

Turbulent viscosity as for $d_m$ = 15 $\mu$m is higher than for $d_m$ = 30 $\mu$m and $d_m$ = 63 $\mu$m, whereby the turbulent viscosity for $d_m$ = 63 $\mu$m is the lowest. This is explained by the different settling behavior of the particles, the height of the available water column to produce turbulence and turbulence damping due to concentration gradients. Finer particles are distributed more over the entire water column, the greater and heavier particles are concentrated at the bottom, see Figure 9. This leads to less turbulence damping in the upper region above $z/h$ = 0.05 for $d_m$ = 30 $\mu$m and $z/h$ = 0.07 for $d_m$ = 63 $\mu$m.

As bottom mud in the simulation with $d_m$ = 15 $\mu$m is lower concentrated than for greater particles, the effective viscosity shows lower values. For the fine material a decrease of effective viscosity is modeled directly at the bed which is due to shear thinning because of high shear rates. In case of coarser material ($d_m$ = 30 $\mu$m and $d_m$ = 63 $\mu$m) the mud layer does not show gradients in the velocity profile and therefore a constant effective viscosity is simulated inside the mud. Since fluid mud shows shear thinning flow behavior, the decrease of effective viscosity at the height of the lutocline seems to be reasonable.

 https://doi.org/10.18171/1.089101

### 3.2.4 Unsteady model performance

Figure 12, Figure 13 and Figure 14 visualize the temporal development of the vertical velocity, the concentration, the turbulent kinetic energy, the dissipation rate, the turbulent and the effective viscosity profiles for $J = 2 \cdot 10^{-5}$, $c_0 = 30$ g/l and $d_m = 35$ $\mu$m. Results for different simulation times $t = 2000$ s, 3000 s, 5000 s, 12000 s, 20000 s are shown. Initial conditions were chosen as $u_0 = 0$, $c_0$ is distributed homogeneously over depth, $k_0 = 0$, $\omega_0 = 0$ and $\nu_{t,0} = 0$.

The concentration shows a sharp transition to high concentrated mud at the bottom, which can be recognized in the velocity profiles (Figure 12), as well. The velocity profiles show no movement of the high concentrated mud layer at the bottom, while the flow is still accelerating. At this stage, the yield stress at the bottom is not exceeded, which would be the condition for flow. The lower concentrated mud above the lutocline starts to flow while forming a non-linear velocity profile. Since the flow is accelerating with time, the mud at the bottom also starts to flow. Starting after $t = 5000$ s, the flow velocity and therefore the sediment diffusion is sufficiently high, so that sediment is resuspended over the whole water depth. This results in a more homogeneous sediment distribution over depth for 12000 s and 20000 s as for earlier simulation times. Upwards diffusion of settled sediment results in a smoothing of the concentration profile.

The corresponding profiles for the turbulent kinetic energy and the dissipation rate $\omega$ are given in Figure 13. The turbulent kinetic energy is zero, when flow velocity is computed to be zero. Immediately over the stationary mud, maximum $k$ is simulated. Greatest values for $k$ are computed when the gradient of the velocity profile is maximum. Since the velocity profile evolves in upward direction with time, a linear distribution of $k$ is only given for steady state ($t = 20000$ s). Peak values of $k$ close to the lutocline explain the erosion of sediment. In this context, sediment transport can be interpreted differently than by exceeding of a critical shear stress. It occurs when chaotic eddies have enough turbulent energy to initiate particle movement. The dissipation rate $\omega$ describes the transformation of smallest eddies into heat. This occurs close to a rigid bottom, when friction is high.

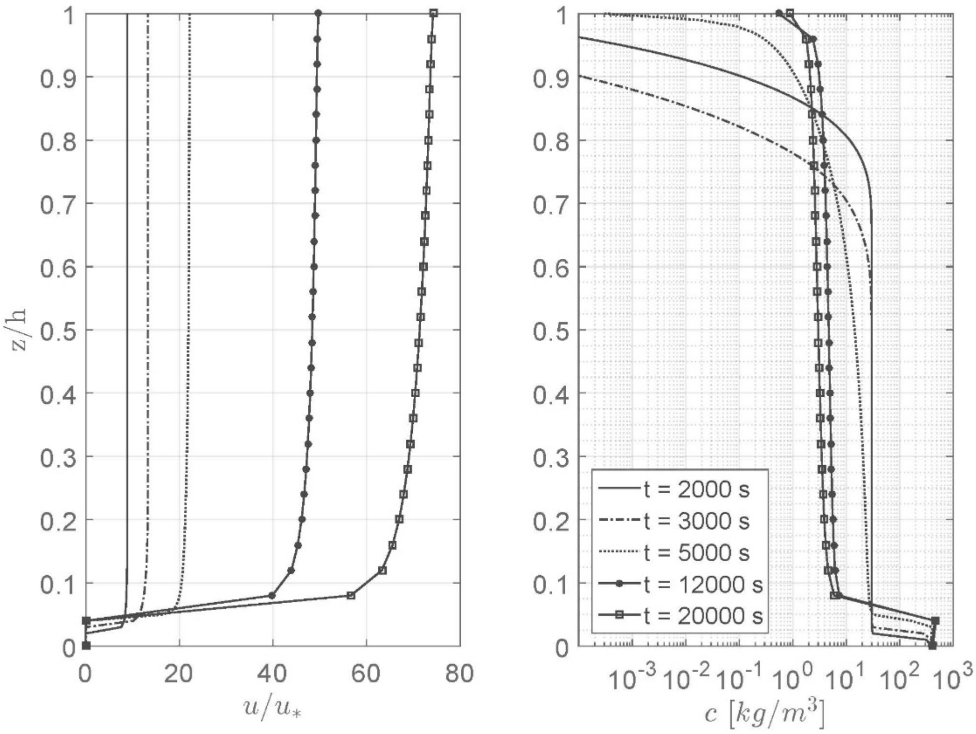


Figure 12: The temporal development of the simulated vertical velocity and concentration profiles are shown. Results are given for $J$ = 2·10⁻⁵, $c_0$= 30 g/l and $d_m$= 35 $\mu$m after different simulation times $t$ = 2000 s, 3000 s, 5000 s, 12000 s, 20000 s. The acceleration of the flow, the formation of bottom and the resuspension of suspended sediment can be regarded.

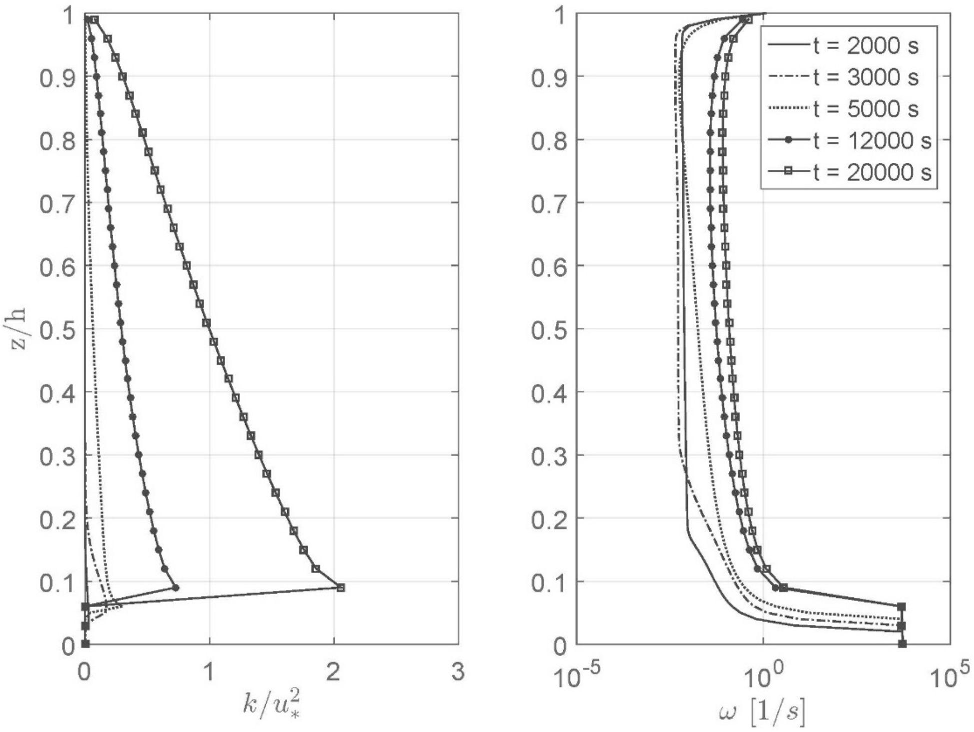


Figure 13: The temporal development of the simulated turbulent kinetic energy and dissipation rate profiles are shown. Results are given for $J$ = 2·10⁻⁵, $c_0$ = 30 g/l and $d_m$= 35 $\mu m$ after different simulation times $t$ = 2000 s, 3000 s, 5000 s, 12000 s, 20000 s. It is shown the evolution of the linear turbulent kinetic energy profiles and the resulting dissipation rate profiles.

Figure 14 describes the temporal development of the turbulent and effective viscosities. Turbulent viscosity profiles show the growth of diffusion, dependent on the evolving velocity and shear rate. The increasing turbulent viscosity is interpreted as an increase of turbulent diffusivity and leads to a smoothing of the concentration profile. Again, the evolution of the profiles starts to develop in upward direction, dependent on the formation of the velocity profile. For zero velocity, $\nu_t$ is zero, as well, as it is shown for $z/h = 0 - 0.08$. At steady state, a parabolic turbulent viscosity profile is simulated, as it is described in literature (Nezu and Nakagawa 1994).

Different formation stages of mobilized and rigid mud are recognized in the effective viscosity. Rigid mud shows high constant rheological viscosities, as the concentration is constant in the formed bottom. While the mud starts to move, the rheological viscosity decreases due to shear thinning. This behavior is dominant at the lutocline which is rising with simulation time. At $t$ = 20000 s the lutocline occurs at $z/h$ = 0.07 and is described by a minimum peak in $\nu_{eff}$. At $t$ = 2000 s and $t$ = 3000 s the effective viscosity is greater in the water column than in vicinity to the bottom. At these simulation times turbulence is zero in the water column due to no shearing, whereby deeper layers start to flow and are forcing a reduction of the effective viscosity close to the bottom. This behavior changes when the velocity profile is developed over the entire water depth and immobile bottom is formed ($t$ = 20000 s).

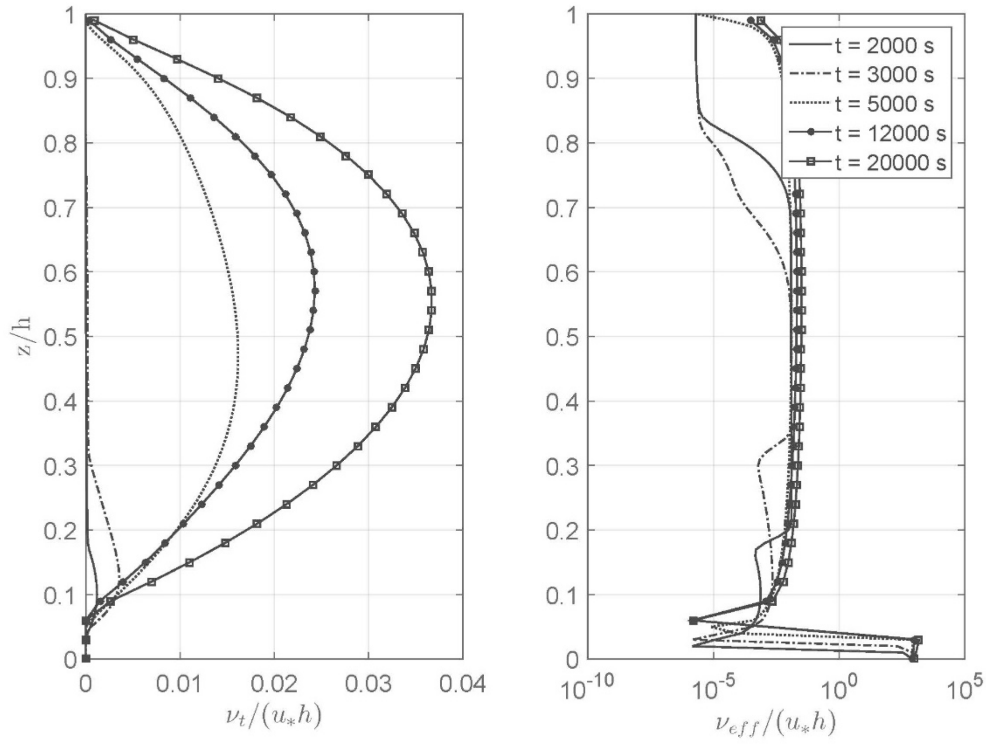


Figure 14: The temporal development of the simulated vertical turbulent viscosity and effective viscosity profiles are shown. Results are given for $J = 2 \cdot 10^{-5}$, $d_m$= 30 g/l and $d_m$= 35 $\mu$m after different simulation times $t$ = 2000 s, 3000 s, 5000 s, 12000 s, 20000 s.

## 4 Conclusions

In this paper a modeling approach is presented, which simulates the water column as well as the fluid mud layer with one set of momentum, transport and turbulence model equations. The model is able to recognize automatically whether the flow is turbulent, laminar or motionless due to high concentrations of suspended matter. In contrast to approaches, which are only valid for the fluid phase, this model is able to consider the fluid and solid phase equally, without distinguishing between different models.

Turbulence is modeled by a modified and new interpreted $k$-$\omega$-turbulence model. Turbulence vanishes automatically inside the mud when no shear rates are present and the turbulence production is zero. Consequently, the turbulence model does not need to be turned off when laminar flow conditions are expected and the turbulent energy equation does not need any changes when mud is formed. In this way a real continuous simulation of water and mud is achieved.

It was found that high mud concentrations lead to a deviation of the logarithmic velocity profile, which was explained by a laminarization of the flow. Furthermore, the creation of a fluid mud layer with a lutocline was reasonably well represented in the model. In the case of highly concentrated mud, the yield stress is not always exceeded, which was shown by simulated zero-velocities.

Nevertheless, a fine spatial discretization is needed, which will affect computational costs when estuarine systems are simulated three-dimensionally. However, the continuous modeling approach is beneficial, since sharp distinctions do not exist between the different processes in river systems. Since the processes are continuously modeled and not separated by coupling different modules for simulating different processes, this approach reduces the influence of empirical uncertainty. The presented model is to be regarded as an improved modeling technique to describe the vertical processes in one set of equations.

Nevertheless, empirical parameters remain such as for the calculation of the settling velocity. The settling velocity appears to be highly sensitive for the formation of fluid mud. Especially when describing hindered settling in high concentrated suspensions parameters need to be validated experimentally.

Future work to improve the computation of turbulence in concentrated mud suspensions is addressed on experimental data for calibration and validation of numerical models. Especially highly resolved measurements of velocity, turbulence and concentration are needed. A verification of cause-effect links is of fundamental importance. Since it is very difficult to achieve natural conditions in the laboratory, there is a clear demand also for further in-situ observations in the field, e.g. estimating turbulent kinetic energy.

## 5 Acknowledgements

The work presented in this paper was part of a joint research project MudEstuary. The MudEstuary project was funded by the German Coastal Engineering Research Council (KFKI) within the German Federal Ministry of Education and Research (BMBF) through the project management of Projektträger Jülich (PTJ) under the grant numbers 03KIS112 and 03KIS113. The funding is gratefully acknowledged.

## 6 Literature

Absi, Rafik; Marchandon, Stéphane; Lavarde, Marc: Turbulent Diffusion of Suspended Particles. Analysis of the Turbulent Schmidt Number. In: DDF, 312-315, 794–799, 2011.

Becker, Marius; Maushake, Christian; Winter, Christian: Observations of Mud-Induced Periodic Stratification in a Hyperturbid Estuary. In: Geophysical Research Letters, 45, 11, 5461–5469. https://doi.org/10.1029/2018gl077966, 2018.

Casulli, Vincenzo: Numerical simulation of three-dimensional free surface flow in isopycnal coordinates. In: International Journal for Numerical Methods in Fluids, 25, 6, 645–658, 1997.

Claus, Betrice; Konermann, Vera: Ems-Ästuar 2030 - Ein Masterplan für die Ems. WWF, 2014.

Coussot, Philippe: Mudflow Rheology and Dynamics: Balkema, 1997.

Crapper, M.; Ali, K.H.M.: A laboratory study of cohesive sediment transport. In: Burt, Neville; Parker, Reg; Watts, Jacqueline (Eds.): Cohesive Sediments: John Wiley Chichester, UK, 197–211, 1997.

Dronkers, Job; van Leussen, Wim: Physical Processes in Estuaries: Springer Science & Business Media, 2012.

Dyer, K. R.; Manning, A. J.: Observation of the size, settling velocity and effective density of flocs, and their fractal dimensions. In: Journal of sea research, 41, 1, 87–95, 1999.

Faas, Richard W.; Wartel, Stanislas I.: Rheological properties of sediment suspensions from Eckernforde and Kieler Forde Bays, Western Baltic Sea. In: International Journal of Sediment Research, 21, 1, 24, 2006.

Knoch, Denise; Malcherek, Andreast: A numerical model for simulation of fluid mud with different rheological behaviors. In: Ocean Dynamics, 61, 2-3, 245–256, 2011.

Kotzé, R.; Haldenwang, R.; Fester, V.; Rossle, W.: In-line rheological characterisation of wastewater sludges using non-invasive ultrasound sensor technology. In: Water SA, 41, 5, 683–690, 2015.

Le Hir, P.; Bassoullet, Ph.; Jestin, H.: Application of the continuous modeling concept to simulate high-concentration suspended sediment in a macrotidal estuary. In: Proceedings in Marine Science, 3, 229–247, 2000.

Le Hir, P.; Cayocca, F.: 3D application of the continuous modelling concept to mud slides in open seas. In: Winterwerp, Johan C.; Kranenburg, Cees (Eds.): Fine Sediment Dynamics in the Marine Environment: Elsevier (Proceedings in Marine Science), 545–562, 2002.

Le Normant, C.: Three-dimensional modelling of cohesive sediment transport in the Loire estuary. In: Hydrological Processes, 14, 13, 2231–2243, 2000.

Le Normant, C.; Lepeintre, F.; Teisson, C.; Malcherek, A.; Markofsky, M.; Zielke, W.: Three dimensional modelling of estuarine processes, MAST Days and Euromar Market. In: Proj. Rep, 1, 1993.

Malcherek, A.; Cha, H.: Zur Rheologie von Flüssigschlicken. Experimentelle Untersuchungen und theoretische Ansätze - Projektbericht. Universität der Bundeswehr München, Institut für Wasserwesen, 2011.

Malcherek, A.; Markofsky, M.; Zielke, W.; Peltier, E.; Le Normant, C.; Teisson, C. et al.: Three Dimensional Numerical Modelling of Cohesive Sediment Transport Processes in Estuarine Environments. Final Report to the EC Contract MAS2-CT92-0013, 1996.

Malcherek, Andreas: Zur Beschreibung der rheologischen Eigenschaften von Flüssigschlicken. In: Die Küste, 77, 135–178, 2010.

Malcherek, Andreas: Sedimenttransport und Morphodynamik. Scriptum – Version 2. Institute of Hydro Sciences, Universität der Bundeswehr München; Universität der Bundeswehr München. Neubiberg, 2016.

McAnally, William H.; Friedrichs, Carl; Hamilton, Douglas; Hayter, Earl; Shrestha, Parmeshwar; Rodriguez, Hugo et al.: Management of Fluid Mud in Estuaries, Bays, and Lakes. I. Present State of Understanding on Character and Behavior. In: J. Hydraul. Eng., 133, 1, 9–22. https://doi.org/10.1061/(asce)0733-9429(2007)133:1(9), 2007.

Migniot, Claude: A study of the physical properties of various very fine sediments and their behaviour under hydrodynamic action, 1968.

Mitchell, S. B.; West, JR: Particle size distribution in an estuarine turbidity maximum region. In: Proceedings in Marine Science, 5, 251–263, 2002.

Nezu, I.; Nakagawa, H.: Turbulence in Open-Channel Flows. In: Journal of Fluid Mechanics, 269, 1994.

Papenmeier, Svenja; Schrottke, Kerstin; Bartholomä, Alexander; Flemming, Burghard W.: Sedimentological and rheological properties of the water-solid bed interface in the Weser and Ems estuaries, North Sea, Germany. Implications for fluid mud classification. In: Journal of Coastal Research, 29, 4, 797–808, 2012.

Richardson, J. F.; Zaki, W. N.: Sedimentation and Fluidization, Part I. In: Trans. Inst. Chem. Eng, 32, 35–53, 1954.

Roland, Aron; Ferrarin, Christian; Bellafiore, Debora; Zhang, Yinglong Joseph; Sikric, Mathieu Dutour; Zanke, Ulrich; Umgiesser, Georg: Über Strömungsmodelle auf unstrukturierten Gitternetzen zur Simulation der Dynamik von Flüssigschlick. In: Die Küste, 79, 2012.

Schrottke, K.: Dynamik fluider Schlicke im Weser und Ems-Ästuar - Untersuchung und Analysen zum Prozessverständnis. In: BAW/BfG Kolloqium, 2006.

Spicer, Patrick T.; Pratsinis, Sotiris E.: Shear-induced flocculation. The evolution of floc structure and the shape of the size distribution at steady state. In: Water Research, 30, 5, 1049–1056, 1996.

Takács, Imre; Patry, Gilles G.; Nolasco, Daniel: A dynamic model of the clarification-thickening process. In: Water Research, 25, 10, 1263–1271, 1991.

Toorman, Erik: Controlled rate concentric cylinder rheometry of estuarine mud suspensions. In: MAST G8M Coastal Morphodynamics Research Project Report (HYD148), 1995.

Toorman, Erik A.: Modelling of turbulent flow with suspended cohesive sediment. In: Winterwerp, Johan C.; Kranenburg, Cees (Eds.): Fine Sediment Dynamics in the Marine Environment, vol. 5: Elsevier (Proceedings in Marine Science), 155–169, 2002.

Uittenbogaard, Robert Eduard; van Kester, J. Th MA; Stelling, Gustaaf Sjoerd: Implementation of Three Turbulence Models in TRISULA for Rectangular Horizontal Grids. Including 2DV-testcases: Delft Hydraulics, 1992.

van Kessel, Thijs; Winterwerp, Han; van Prooijen, Bram; van Ledden, Mathijs; Borst, Wil: Modelling the seasonal dynamics of SPM with a simple algorithm for the buffering of fines in a sandy seabed. In: Continental Shelf Research, 31, 10, 124–134, 2011.

van Rijn, Leo C.: Principles of Sediment Transport in Rivers, Estuaries and Coastal Seas. Edited by AQUA Publications, 1993.

Violet, P. L.: On the Numerical Modelling of Stratified Flows. In: Physical Processes in Estuaries, 1988.

Wehr, Denise: An Isopycnal Numerical Model for the Simulation of Fluid Mud Dynamics. Universität der Bundeswehr München - Institut für Wasserwesen, 2012.

Wells, John T.; Coleman, James M.: Physical processes and fine-grained sediment dynamics, coast of Surinam, South America. In: Journal of Sedimentary Research, 51, 4, 1981.

Wentworth, Chester K.: A scale of grade and class terms for clastic sediments. In: The Journal of Geology, 377–392, 1922.

Whitehouse, Richard; Soulsby, Richard; Roberts, William; Mitchener, Helen: Dynamics of Estuarine Muds: Thomas Telford, 2000.

Wilcox, David C.: Turbulence Modeling for CFD: DCW Industries, Inc., 1994.

Winterwerp, J. C.: On the flocculation and settling velocity of estuarine mud. In: Continental Shelf Research, 22, 9, 1339–1360, 2002.

Winterwerp, J. C.; Bruens, A. W.; Gratiot, Nicolas; Kranenburg, C.; Mory, M.; Toorman, E. A.: Dynamics of concentrated benthic suspension layers. In: Proceedings in Marine Science, 5, 41–55, 2002.

Worrall, W. E.; Tuliani, S.: Viscosity changes during the ageing of clay-water suspensions. In: Trans Brit Ceramic Soc, 63, 167–185, 1964.